HIGH POWER LASER
SCIENCE AND ENGINEERING

RESEARCH ARTICLE

A continuous-wave Nd:YVO$_4$-KGW intracavity Raman laser with over 34% diode-to-Stokes optical efficiency

Quan Sheng [1,2], Jingni Geng [1,2], Tianchang Liu[1,2], Shijie Fu[1,2], Wei Shi[1,2], and Jianquan Yao[1,2]

[1]*Institute of Laser and Optoelectronics, School of Precision Instrument and Optoelectronics Engineering, Tianjin University, Tianjin, China*

[2]*Key Laboratory of Optoelectronic Information Technology (Ministry of Education), Tianjin University, Tianjin, China*

Abstract

We demonstrate a continuous-wave (CW) Nd:YVO$_4$-potassium gadolinium tungstate (KGW) intracavity Raman laser with a diode-to-Stokes optical efficiency of 34.2%. By optimizing the cavity arrangement and reducing the cavity losses, 8.47 W Stokes output at 1177 nm was obtained under an incident 878.6 nm diode pump power of 24.8 W. The influence of cavity losses on the power and efficiency of the CW Raman laser, as well as the potential for further optimization, was investigated based on the numerical model. The observation of thermally-induced output rollover was well explained by the calculation of the thermal lensing and cavity stability, indicating that the end-face curvature played an important role when the end-face of the crystal was highly reflective coated to make the cavity. A 10.9 W Stokes output under 40.9 W incident pump was also demonstrated with a cavity arrangement less sensitive to the end-face curvature, which is the highest output power of CW intracavity Raman lasers reported.

Keywords: continuous wave; intracavity Raman laser; KGW crystal; thermal lens

1. Introduction

Solid-state Raman lasers based on stimulated Raman scattering (SRS) in crystalline Raman gain media have been established as reliable laser sources for wavelength regions that are difficult to obtain directly with population inversion lasers[1,2]. Benefiting from the automatic phase matching and beam clean-up characteristics of the SRS process, Raman lasers can generate output in the whole transparent range of the gain media with good beam quality. Combined with the second harmonic generation (SHG) and/or sum-frequency generation (SFG) techniques, Raman lasers with output from ultraviolet to mid-infrared have been demonstrated with various Raman crystals, including tungstate, vanadate, nitrate and niobate, as well as the recently developed diamond, which benefits from a very high Raman gain coefficient, damage threshold and thermal conductivity[3–9].

As a third-order nonlinear process, the SRS gain relies on the high fundamental laser intensity significantly.

For continuous-wave (CW) Raman lasers, tens of watts fundamental laser powers are usually required to reach the SRS threshold[8], despite the tightly focused and double-pass pump scheme being utilized. Therefore, an intracavity pump scheme (including the self-Raman scheme) is preferred in low-to-moderate power CW Raman lasers. Incorporating the Raman gain medium inside the fundamental laser cavity to make use of high intracavity powers, efficient CW Raman conversion can be realized under watt-level laser diode (LD) pump power[10–12]. Multi-watt CW near-infrared Stokes output and versatile visible harmonic output from intracavity Raman lasers have been demonstrated by several research groups[10–13].

One main issue that limits the power and efficiency scaling of CW Raman lasers is the cavity losses. Most CW Raman lasers have output coupling at the level of 1%–2% or lower (including those with high-Q Stokes cavity and intracavity SHG/SFG nonlinear coupling for visible output) because of the low gain. Therefore, even tiny passive Stokes cavity losses would decrease the slope efficiency and increase the threshold of the laser seriously. The fundamental cavity losses would also weaken the coupling from the fundamental field to the Stokes wave. A comprehensive model on the efficiency of CW intracavity Raman lasers

Correspondence to: Shijie Fu and Wei Shi, School of Precision Instrument and Optoelectronics Engineering, Tianjin University, Tianjin 300072, China. E-mail: shijie_fu@tju.edu.cn (S. Fu); shiwei@tju.edu.cn (W. Shi)

has been presented by Spence *et al.*[14,15]. Based on their model, decreasing the round-trip losses of the fundamental and Stokes fields from 1% to 0.5% may increase the optical efficiency of the Raman laser from 18% to 39%. In 2016, Fan *et al.*[10] reported a self-Raman laser based on a YVO$_4$/Nd:YVO$_4$/YVO$_4$ crystal. With the self-Raman scheme minimizing the insertion losses, they obtained 5.3 W CW Stokes output at 1176 nm with an optical efficiency of 20%. In 2021, Chen *et al.*[13] demonstrated a frequency-doubled CW Nd:GdVO$_4$-potassium gadolinium tungstate (KGW) intracavity Raman laser. With a high-reflection (HR) mirror being optimized to decrease the non-unity reflection losses of the fundamental and Stokes waves, the quasi-continuous-wave (QCW) yellow output power was improved significantly from 5.7 to 10.5 W, with conversion efficiency increased from 15% to 26.3%.

Another issue is the strong thermal lensing that occurs in both the laser and Raman crystals at high pump levels[13,16]. For example, the yellow Raman laser in Ref. [13] could deliver 10.5 W instantaneous QCW output when operating with a 50% pump duty circle to alleviate the thermal load, but the maximum output power in the CW scheme was limited to 4.5 W because of the thermal lensing. Therefore, determining the strength of thermal lensing and making corresponding compensation via cavity design is essential for high-power Raman laser output.

In this work, we demonstrated an efficient CW Nd:YVO$_4$-KGW intracavity Raman laser. To minimize the cavity losses, we used a KGW Raman crystal with HR Stokes coating on one of its end-faces to remove the necessity of the separated dichroic mirror that is usually used. With this design, the efficiency of the Raman laser was improved significantly compared with that using a separated dichroic mirror to make the Stokes cavity. An 8.47 W CW Stokes output at 1177 nm was obtained under an incident LD pump power of 24.8 W, with the optical efficiency being 34.2%, which is the highest efficiency of CW intracavity Raman lasers reported. The influence of cavity losses on the power and efficiency of the Raman laser was analyzed based on the rate equation model. Besides, we found that the influence of thermal lensing on cavity stability differed significantly with the two Stokes cavity arrangements, because the thermally-induced end-face curvature played different roles.

The detailed calculation of the thermal lensing and cavity stability explained the experimental observation well.

2. Experimental arrangement

Figure 1 depicts the experimental arrangement. The pump source was a fiber-coupled wavelength-stabilized LD at 878.6 nm with a maximum power of 65 W, a fiber core diameter of 400 μm and a numerical aperture of 0.22. The pump light was focused onto the input face of an *a*-cut Nd:YVO$_4$ crystal used as the gain medium of the 1064 nm fundamental laser with a spot radius of 280 μm. The 3 mm × 3 mm × 15 mm Nd:YVO$_4$ crystal (CASTECH, Inc.) with a doping concentration of 0.2% (atomic fraction) absorbed approximately 80% of the incident random polarized pump light. The folded cavity of the 1064 nm fundamental laser was defined by a flat HR mirror M1, a concave HR mirror M2 with a radius of curvature (RoC) of 100 mm and a concave HR mirror M3 with an RoC of 200 mm. Mirror M3 also served as the Stokes output coupler, with a transmittance of $T_S = 0.7\%$ at 1177 nm. The distances M1–M2 and M2–M3 were 168 and 65 mm, respectively. The folding angle was set as small as possible to be 25° (full angle) to minimize the influence of astigmatism. A 3 mm × 3 mm × 20 mm KGW crystal cut along its N_p-axis (CASTECH, Inc.) was used as the Raman gain medium. The laser and Raman crystals were oriented to have the 1064 nm fundamental laser polarized along the N_m-axis of the KGW crystal, to make use of the strong 901 cm^{-1} Raman gain for 1177 nm Stokes output while suppressing the 768 cm^{-1} Raman line and cascaded Raman conversions[17]. The Nd:YVO$_4$ crystal and KGW crystal were wrapped in indium foil and mounted in aluminum holders water cooled at 20°C, and located close to mirrors M1 and M3, respectively.

In the experiment, we tried two different Stokes cavity arrangements. To minimize the fundamental and Stokes cavity losses L_F and L_S, which may limit the laser efficiency seriously, we used a KGW crystal with 1064 nm anti-reflection (AR) coating on both faces (marked as SC1 and SC2 in Figure 1) and 1177 nm HR coating on one face (SC1), to remove the necessity of an additional dichroic mirror M4 (AR@1064 nm on both of its faces, SM41 and SM42,
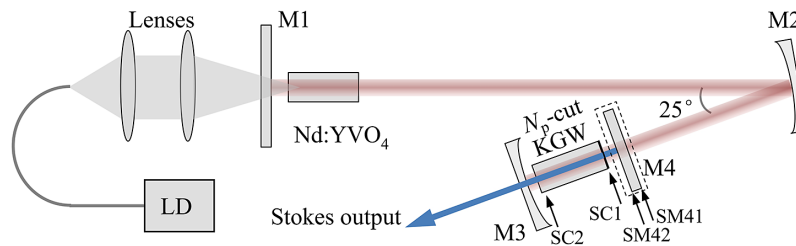
Figure 1. Experimental setup of the Nd:YVO$_4$-KGW intracavity Raman laser with Stokes HR coating on one of the crystal end-faces and on a separate mirror.

Table 1. The reflectivities of the AR coatings and transmittances of the HR coating of each surface provided by the manufacturers.

Cavity arrangement with HR mirror M4			Cavity arrangement with HR coating on KGW		
Surfaces	1064 nm	1177 nm	Surfaces	1064 nm	1177 nm
SC1	$R = 0.144\%$	$R = 0.22\%$	SC1	$R = 0.54\%$	$T = 0.03\%$
SC2	$R = 0.36\%$	$R = 0.23\%$	SC2	$R = 0.33\%$	$R = 0.12\%$
SM41	$R = 0.01\%$	/			
SM42	$R = 0.16\%$	$T = 0.037\%$			
Sum of the unwanted R and T for a round-trip	1.55%	0.94%	Sum of the unwanted R and T for a round-trip	1.94%	0.27%

and HR@1177 nm on one face SM42, from CRYSTECH, Inc.) for the Stokes cavity. For comparison, we also used a KGW crystal with AR coatings at both 1064 and 1177 nm on both faces and the separate dichroic mirror M4 to make the Stokes cavity with the output coupler M3. The Stokes cavity lengths were 22 mm for the case with HR coating on crystal and 23 mm when using the separate HR mirror M4. Table 1 gives the reflectivities of the AR coatings and transmittances of the HR coating of each surface provided by the manufacturers, which are different for the two cavity arrangements. Other unchanged elements, including M1, M2, M3 and the Nd:YVO$_4$ crystal, brought a total round-trip loss of 0.2% to the fundamental laser. For the case with the Stokes HR coating on the crystal end-face SC1, the sum of the unwanted reflectivities and transmittances of the 1064 nm fundamental laser cavity for a round-trip was 1.94%, comparable to that of 1.55% when using the separate HR mirror M4 to make the Stokes cavity. However, the sum of the unwanted reflectivities and transmittances for the Stokes wave in its cavity was reduced significantly from 0.94% to 0.27%. Considering the rather low Stokes output coupling of 0.7%, reducing the Stokes cavity loss may help to enhance the Raman laser efficiency significantly.

3. Experimental results

Figure 2 shows the output power of the 1177 nm Stokes wave (P_{S_out}) as a function of the incident LD pump power (P_P), measured using a laser powermeter, Ophir VEGA, with a sensor, 30A-BB-18. The 1064 nm leakage power recorded behind the mirror M2 is also plotted in the figure. We can see that with the Stokes cavity losses reduced by removing the separate dichroic mirror M4, the Raman laser with the KGW crystal HR coated for Stokes wave exhibited a lower SRS threshold and an enhanced conversion efficiency (black dot) compared with the case with an AR-coated crystal and a dichroic mirror. With the same $T_S = 0.7\%$ Stokes output coupler, the SRS threshold was decreased from 4.3 to 2.2 W incident LD power. The Stokes output power reached 8.47 W under the incident pump power of 24.8 W, with optical efficiency and slope efficiency being 34.2% and 38.6%, respectively. To the best of our knowledge, this is the first
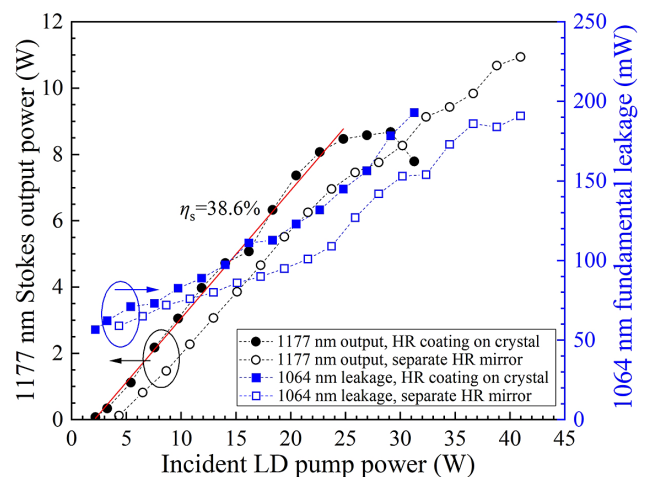
Figure 2. Stokes output power and fundamental laser leakage as a function of incident LD pump power, with the two different cavity arrangements.

demonstration of a CW intracavity Raman laser with optical efficiency over 30%, which is mainly attributed to the cavity design optimized for mode-matching and reduction of cavity losses. Note that the Nd:YVO$_4$ crystal absorbed only 80% of the incident pump, and the conversion efficiency with respect to absorbed pump power reached 42.8%. However, the increase of Stokes output power became quite slow thereafter, and finally rolled over when the pump power exceeded 29.1 W (with Stokes output power of 8.68 W).

For comparison, when using the separate dichroic mirror M4, the Stokes output powers (black empty circle) were much lower than those with the HR-coated KGW under the same pump power below 27 W, due to the higher Stokes cavity losses. Nevertheless, the rollover did not occur with this cavity arrangement even at the maximum pump power used in the experiment of 40.9 W. A maximum Stokes output power of 10.9 W was obtained, with the optical efficiency being 26.6%. This is the highest output power of CW crystalline Raman lasers with gain media besides the newly developed diamond crystal, including both intracavity and extracavity schemes. We did not further increase the pump power considering the risk of component damage given the high circulating power in the cavity.
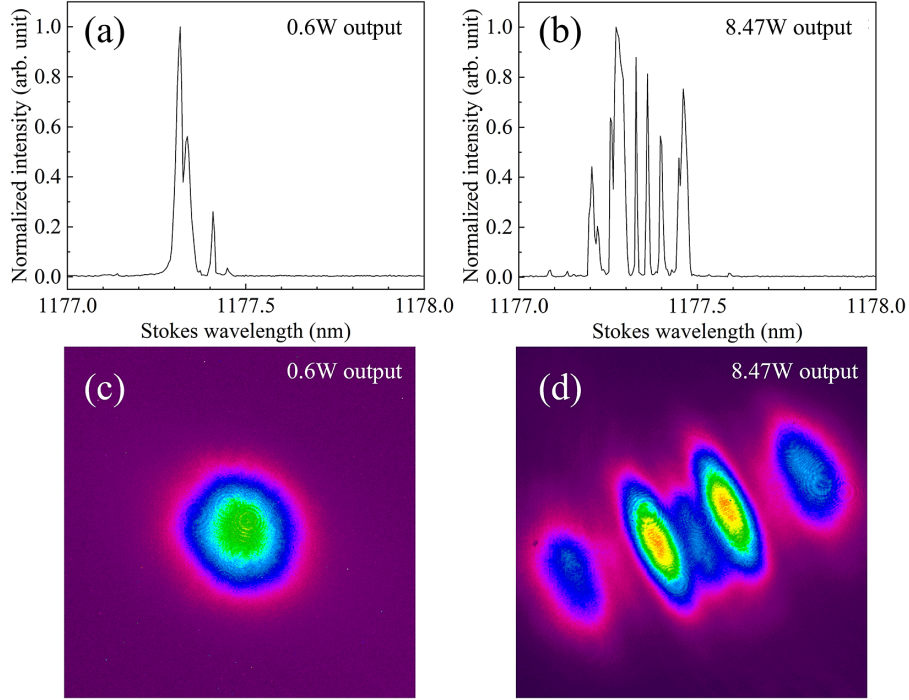
Figure 3. Typical Stokes spectra (a), (b) and beam profiles (c), (d) at different Stokes output powers, with the HR-coated KGW crystal.

Figure 3 shows some typical spectra and beam profiles, recorded using an optical spectrum analyzer, Yokogawa 6370D (resolution 0.02 nm), and a charge-coupled device (CCD) camera, SP907, respectively. The Stokes spectra broadened with the increasing pump power, and were multi-line with linewidths of approximately 0.3 nm at the maximum pump. Compared with our previous work in which a $T_S = 0.4\%$ output coupler was used[17], neither cascaded Raman lines nor second Stokes lines were observed here, since the higher output coupling of $T_S = 0.7\%$ decreased the intracavity Stokes power. The Stokes beam profile became elliptic when the output power was over 5 W because of the astigmatic thermal lens in the KGW crystal and finally reached the multi-lobe high-order Hermite–Gaussian mode[16].

4. Discussion

4.1. Stokes power/efficiency and cavity losses

The experimental results showed that the efficiency of the Raman laser was quite sensitive to the cavity losses. The influence of cavity losses on the power/efficiency of the Raman laser was then estimated based on the model presented by Spence[15], with backward Raman gain taken into consideration for the CW operation scheme. With the thermal lens in the crystal considered, the average TEM_{00} mode beam radii of the 1064 nm fundamental laser in the Nd:YVO$_4$ crystal and the KGW crystal were calculated to be 270 and 80 μm, respectively, while the TEM_{00} mode beam radius of

the Stokes field in the KGW crystal was 110 μm. Considering the fundamental laser usually operates in multi-transverse mode when intracavity SRS occurs, the fundamental beam radius at the KGW crystal used in the power/efficiency simulation was 110 μm. The Raman gain coefficient of the KGW crystal used in the calculation was 3 cm/GW rather than the steady-state Raman gain coefficient of 4.5 cm/GW for a 1064 nm fundamental laser polarized along the N_m-axis, with the influence of fundamental and Stokes spectral broadening on the effective Raman gain considered[15].

Figure 4 plots the calculated optical efficiency P_{S_out}/P_P of the intracavity Raman laser as a function of the fundamental and Stokes round-trip losses. As shown in Figure 4(a), for the case using the KGW crystal with HR Stokes coating, the calculated optical efficiency of 32.6% under the pump power of 24.8 W matched very well with the experimental result of 32.4%. From the figure we can see that reducing the Stokes cavity losses is critical for optimizing the laser efficiency, because of the low output coupling. Besides, if round-trip losses of the fundamental laser L_F can be reduced to 0.5% or lower, the optical efficiency of the CW intracavity Raman laser can be further improved to the level of 40%–45%. For the separate dichroic mirror cavity arrangement with round-trip losses of $L_F = 1.55\%$ and $L_S = 0.94\%$ for fundamental and Stokes waves, respectively, the calculated optical efficiency was 20.4% under a 40.9 W pump (Figure 4(b)), lower than the experimental value of 26.6%. This reveals that the actual round-trip losses may be lower than those calculated by adding up the unwanted reflectivities and transmittances provided by the element
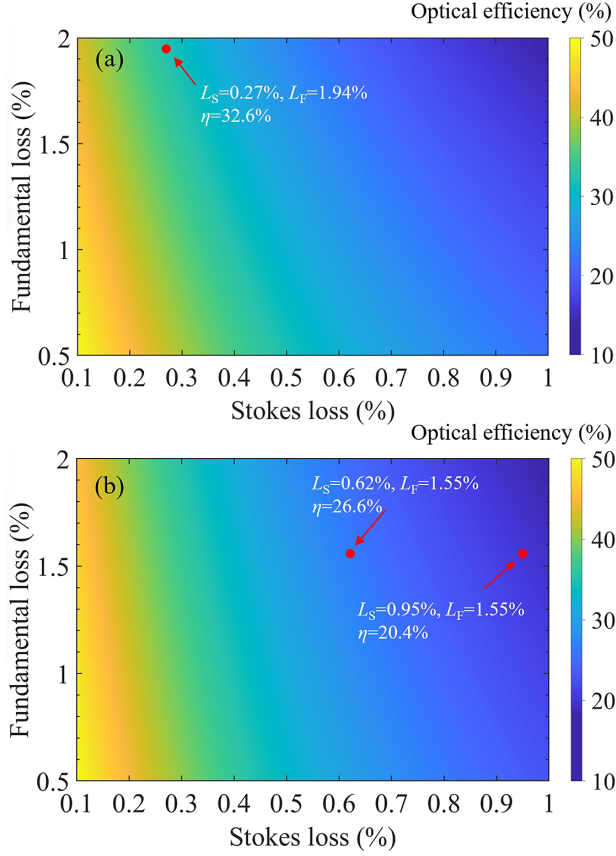
Figure 4. Optical efficiency P_{S_out}/P_P of the Raman laser as a function of the Stokes and fundamental round-trip losses, with the incident pump power of (a) 24.8 W and (b) 40.9 W, respectively. The calculation used a 270-μm fundamental laser radius in the laser crystal, 110-μm fundamental laser radius and Stokes beam radius in the KGW crystal and 0.7% output coupling for the Stokes wave.

manufacturers in Table 1. For example, in this arrangement with the separated dichroic mirror M4, the calculated Stokes losses L_S mainly came from the coatings on the two faces of the KGW crystal with quite similar reflectivities. The actual (single-pass) loss may be lower than the sum of the two due to the weak etalon effect between the two parallel surfaces. Considering that the influence of L_F is not as significant as that of the Stokes loss, the deviation between the calculated and experimental values was mainly due to the overestimated L_S. Assuming an L_F of 1.55%, the L_S should be approximately 0.62% (including the nonnegligible absorption loss induced by the Tm^{3+} impurity, which caused the strong blue fluorescence[18]) for the experimental optical efficiency of 26.6% under incident pump power of 40.9 W.

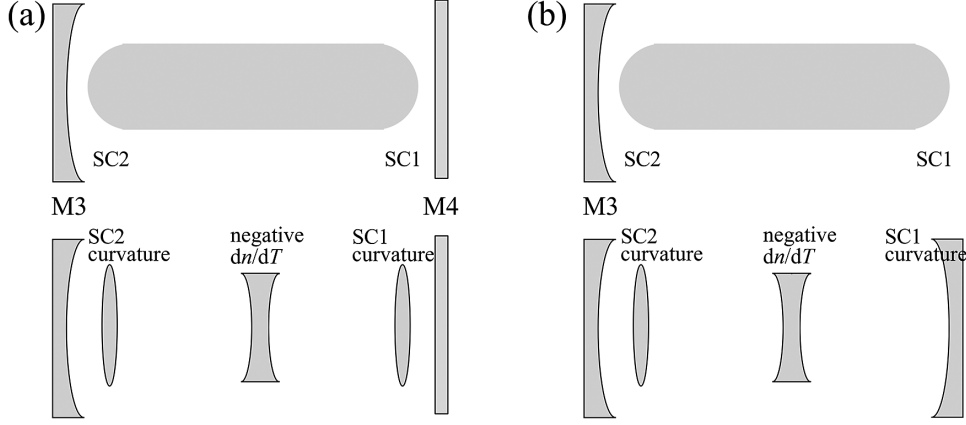### 4.2. Influence of the KGW crystal end-face curvature

It was interesting that the maximum Stokes output powers before rollover were quite different with the two cavity arrangements. In fact, we also tried output couplers with

transmittances of 0.4% and 1.1% in the experiment. With all these output couplers, the rollover of Stokes output power occurred much earlier when using the HR-coated KGW crystal than that with the separate dichroic mirror M4. We can see from Figure 2 that the 1064 nm leakage behind the folding mirror M2 (blue solid square) kept growing after the rollover of the Stokes output occurred, revealing that the rollover was due to the stability issue of the Stokes cavity, rather than that of the fundamental laser cavity.

The only difference between the two Stokes cavity arrangements is the dichroic mirror M4 used to make the Stokes cavity being replaced by the HR coating on the KGW crystal. In these two arrangements, the influences of thermally-induced end-face curvature of the surface SC1 on the cavity stability are different. Different from conventional single-end-pumped inversion lasers, the SRS thermal load in the KGW crystal was distributed uniformly along the crystal length. As shown in Figure 5(a), the negative thermo-optic coefficient dn/dT of the KGW crystal induced strong negative thermal lensing f_{tn}, which can be seen as a thin lens in the middle of the crystal. By contrast, the end-face curvature due to the thermal expansion introduced positive thermal lensing f_{te} at both end-faces. In this case, the *ABCD* matrix of SC1-M4-SC1 (which goes through the end-face SC1 twice) is [1, 0; −2/f_{te}, 1], when neglecting the small distance of approximately 1 mm between the crystal and the mirror M4. The f_{te} here is the thermal lens focal length of the single curved end-face induced by thermal expansion. For the case with HR Stokes coating on the KGW crystal, as shown in Figure 5(b), the SC1-M4-SC1 is replaced by a concave reflecting surface SC1 with an *ABCD* matrix of [1, 0; −1/(R_e/2), 1], where R_e is the thermal-expansion-induced RoC of the end-face SC1, with its relationship with f_{te} being $R_e = 2f_{te}(n−1)$[19], where n is the refractive index of the crystal ($n = 1.99$ for 1177 nm Stokes power polarized along the N_m-axis of the KGW crystal). For the KGW crystal with a large negative dn/dT, it is the strong negative thermal lensing that makes the Stokes cavity unstable, while the positive end-face curvature would compensate for the negative thermal lensing to some extent[20]. When using the separate dichroic mirror M4 to make the Stokes cavity with output coupler M3, the oscillating beam passed through the focusing surface SC1 twice, therefore experiencing stronger positive thermal lensing compared with the case using the HR-coated KGW crystal, so that the negative thermal lensing was compensated more and allowed the laser to operate with higher Stokes power.

The thermal lens focal length induced by the thermo-optic coefficient and end-face curvature of the Raman crystal KGW can be estimated using the following equations[19,20]:

$$f_{tn} = \frac{k_C \pi w_S^2}{P_h} \left(\frac{dn}{dT} \right)^{-1}, \quad (1)$$

Figure 5. Schematic of the influences of the end-face curvature on the cavity scheme.

$$f_{\text{te}} = \frac{k_C \pi w_S^2}{P_h} \left(\frac{\alpha r_0 (n-1)}{l} \right)^{-1}, \qquad (2)$$

where k_C is the thermal conductivity, w_S is the Stokes beam radius, α is the thermal expansion coefficient, r_0 is the radius of the crystal end-face, l is the crystal length and $P_h = P_S(\lambda_S/\lambda_L - 1)$ is the heat generated, in which λ_S and λ_L are the Stokes and fundamental wavelengths, respectively. Note that the P_S in the equations is the Stokes power generated rather than the output power from the output coupler P_{S_out}, with the relationship $P_{S\_out} = P_S \times T_S/(T_S + L_S)$. For the Stokes cavities with HR-coated KGW crystal and separated dichroic mirror M4 here, the P_S values are 1.39 and 1.89 times those of P_{S_out}, respectively. For the N_p-cut KGW crystal with the laser polarized along its N_m-axis, we have $dn/dT = -0.8 \times 10^{-6}$ K^{-1}, $k_C = 3.4$ W/(m·K) and $\alpha = 1.6 \times 10^{-6}$ K^{-1}[21].

Figure 6 plots the calculated negative f_{tn} and positive f_{te} as a function of the generated Stokes power. Both of them became stronger with the increasing Stokes power. The f_{tn} values are −343, −171.5 and −114.4 mm, respectively, with 5, 10, and 15 W Stokes power generated, while the f_{te} values are 2174, 1087 and 725 mm. The gradients of the lens strength with respect to the generated Stokes power are 0.58 and 0.092 D/W, respectively. With the relationship between f_{tn} and f_{te} determined, we can further calculate their influence on the cavity stability with the two different Stokes cavity arrangements depicted in Figure 5, as shown in Figure 7. With the HR-coated KGW crystal, the cavity would become unstable with a negative f_{tn} shorter than −155 mm, while the f_{te} is 972 mm. For the Stokes cavity with the separate dichroic mirror M4, the positive f_{te} compensates more on the negative f_{tn}, and the cavity allows the f_{tn} as short as −135 mm (with the corresponding f_{te} being 856 mm). The calculation results could well explain why the rollover of Stokes power occurred earlier when using the HR-coated KGW crystal
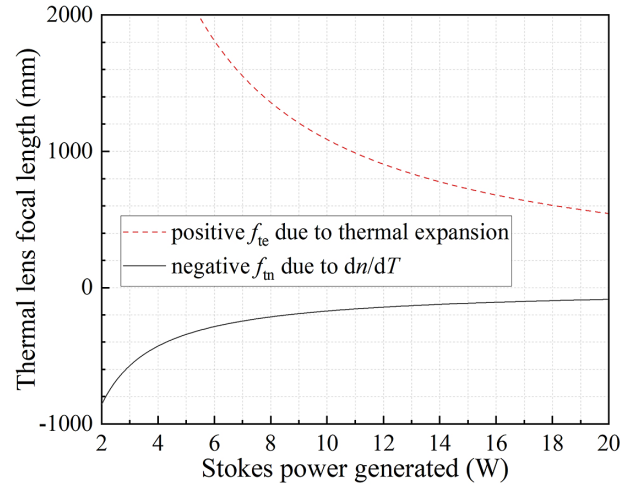
Figure 6. Thermo-optically induced negative thermal lens focal length and (single) end-face curvature induced positive thermal lens focal length as a function of Stokes power generated in the KGW crystal, in p[mm]p orientation. The fundamental and Stokes wavelengths are 1064 and 1177 nm, respectively. The Stokes beam radius in the KGW crystal used in the calculation is 110 μm.

than with the separate M4, despite the contribution of the photoelastic effect being neglected in the calculation. Moreover, the fundamental mode beam size of the Stokes wave would expand significantly before the cavity became unstable. The astigmatic thermal lensing in the KGW crystal also makes the Stokes field operate in high-order transverse mode[16]. These issues may weaken the thermal lensing to some extent. Considering the current limitation of Stokes cavity stability on output power with the HR-coated KGW crystal, one can use the output coupler M3 with a smaller RoC that allows stronger negative thermal lensing for higher power.

From Figure 4 we know that the optical efficiency of the CW intracavity Raman laser could reach 40% or higher with proper control of cavity losses and output coupling. The KGW crystal is capable of generating a tens of watts output with very good beam quality when serving as the
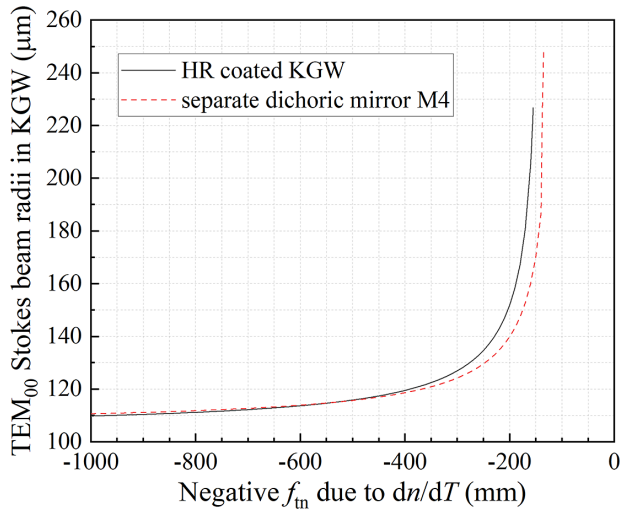
Figure 7. TEM$_{00}$ mode Stokes beam size evolution with thermo-optically induced f_{tn} in the KGW crystal with the two different cavity arrangements, with the relationship between f_{tn} and f_{te} considered.

host of inversion laser gain media, with cavity design well compensating for the strong astigmatic thermal lensing[22]. Therefore, we can expect 20–30 W CW output from such end-pumped intracavity Raman lasers with conventional Raman crystals, such as KGW. It should be mentioned that this level of output power is still one to two orders of magnitude lower than those of the state-of-the-art extracavity diamond Raman lasers, with which 154 W CW output and 1.2 kW QCW peak power have been demonstrated by virtue of the superior thermal properties and Raman gain of the diamond crystal[23,24]. However, the intracavity approaches with cheap and easily accessible conventional Raman crystals still provide a very efficient and low-threshold choice for versatile output wavelengths with 10-W or higher power under low-to-moderate primary pump power.

5. Conclusion

In conclusion, we have demonstrated an efficient CW Nd:YVO$_4$-KGW intracavity Raman laser. By using a Raman crystal with one of its end-faces coated for HR at the Stokes wavelength to remove the dichroic mirror and reduce the cavity losses, 8.47 W Stokes output at 1177 nm was obtained under the incident pump power of 24.8 W, with optical efficiency being 34.2%, which is the highest among CW intracavity Raman lasers reported. The influence of cavity losses on the power and efficiency of the Raman laser was investigated based on the numerical model. Besides, it was observed that the output rollover related to thermal lensing is quite different for Stokes cavities with an HR-coated crystal end-face and with a dichroic mirror as the total reflector. The calculation on the thermal lensing and cavity mode revealed that the thermally-induced end-face curvature of the KGW crystal has different effects on the cavity stability with the two cavity arrangements.

References

1. R. Casula, J. Penttinen, M. Guina, A. J. Kemp, and J. E. Hastie, Optica **5**, 1406 (2018).
2. H. M. Pask, P. Dekker, R. P. Mildren, D. J. Spence, and J. A. Piper, Prog. Quantum. Electron. **32**, 121 (2008).
3. N. Gelbach, Y. Neustadter, M. Henig, R. Nahear, and S. Noach, Opt. Lett. **48**, 4444 (2023).
4. Q. Sheng, A. J. Lee, D. J. Spence, and H. M. Pask, Opt. Express **26**, 32145 (2018).
5. Y. Duan, Y. Sun, H. Zhu, T. Mao, L. Zhang, and X. Chen, Opt. Lett. **45**, 2564 (2020).
6. H. Zhao, C. Lin, C. Jiang, S. Dai, H. Zhou, S. Zhu, H. Yin, Z. Li, and Z. Chen, Opt. Express **31**, 265 (2023).
7. A. M. Warrier, J. Lin, H. M. Pask, A. J. Lee, and D. J. Spence, Opt. Express **23**, 25582 (2015).
8. Z. Bai, R. J. Williams, O. Kitzler, S. Sarang, D. J. Spence, and R. P. Mildren, Opt. Express **26**, 19797 (2018).
9. Y. Liu, C. Zhu, Y. Sun, R. Mildren, Z. Bai, B. Zhang, and Y. Feng, High Power Laser Sci. Eng. **11**, e72 (2023).
10. L. Fan, W. Zhao, X. Qiao, C. Xia, L. Wang, H. Fan, and M. Shen, Chin. Phys. B **25**, 114207 (2016).
11. Q. Sheng, R. Li, A. J. Lee, D. J. Spence, and H. M. Pask, Opt. Express **27**, 8540 (2019).
12. Y. C. Liu, C. M. Chen, J. Q. Hsiao, Y. Y. Pan, C. H. Tsou, H. C. Liang, and Y. F. Chen, Opt. Lett. **45**, 1144 (2020).
13. Y. F. Chen, D. Li, Y. M. Lee, C. C. Lee, H. Y. Huang, C. H. Tsou, and H. C. Liang, Opt. Lett. **46**, 797 (2021).
14. D. J. Spence, P. Dekker, and H. M. Pask, IEEE J. Sel. Topics Quantum Electron. **13**, 756 (2007).
15. D. J. Spence, IEEE J. Sel. Topics Quantum Electron. **21**, 1400108 (2015).
16. A. McKay, O. Kitzler, and R. P. Mildren, Opt. Express **22**, 6707 (2014).
17. J. Geng, Q. Sheng, S. Fu, W. Shi, and J. Yao, Opt. Lett. **48**, 6364 (2023).
18. J. Neto, C. Artlett, A. Lee, J. Lin, D. Spence, J. Piper, N. Wetter, and H. Pask, Opt. Mater. Express **4**, 889 (2014).
19. W. Koechner, *Solid-State Laser Engineering*, 6th ed., Springer Series in Optical Sciences (Springer, 2006).
20. H. M. Pask, Prog. Quantum. Electron. **27**, 3 (2003).
21. I. V. Mochalov, Opt. Eng. **36**, 1660 (1997).
22. Z. Tu, J. J. Guo, Z. Gan, Z. Gao, Y. Gao, Y. Huang, W. Guo, and X. Liang, Opt. Lett. **48**, 6263 (2023).
23. R. J. Williams, O. Kitzler, Z. Bai, S. Sarang, H. Jasbeer, A. McKay, S. Antipov, A. Sabella, O. Lux, D. J. Spence, and R. P. Mildren, IEEE J. Sel. Top. Quant. **24**, 1602214 (2018).
24. S. Antipov, A. Sabella, R. J. Williams, O. Kitzler, D. J. Spence, and R. P. Mildren, Opt. Lett. **44**, 2506 (2019).